# Three-dimensional computed tomography mapping and clinical predictive factors for morphologic characterization of displaced femoral neck fractures

**Shenghui Wu[1#^], Xiaozhong Zhu[1#^], Wei Wang[2^], Yingqi Zhang[3^], Guangyi Li[1^], Jiong Mei[1^]**

[1]Department of Orthopedic Surgery, Shanghai Sixth People's Hospital Affiliated to Shanghai Jiao Tong University School of Medicine, Shanghai, China; [2]Department of Biomedical Engineering, The Hong Kong Polytechnic University, Hong Kong, China; [3]Department of Orthopedic Surgery, Tongji Hospital, Tongji University School of Medicine, Shanghai, China

*Contributions:* (I) Conception and design: S Wu, J Mei; (II) Administrative support: Y Zhang, J Mei; (III) Provision of study materials or patients: S Wu, X Zhu; (IV) Collection and assembly of data: S Wu, X Zhu; (V) Data analysis and interpretation: W Wang, Y Zhang, G Li; (VI) Manuscript writing: All authors; (VII) Final approval of manuscript: All authors.

[#]These authors contributed equally to this work.

*Correspondence to:* Jiong Mei, MD. Department of Orthopedic Surgery, Shanghai Sixth People's Hospital Affiliated to Shanghai Jiao Tong University School of Medicine, No. 600 Yishan Road, Shanghai 200233, China. Email: meijiong@sjtu.edu.cn.

**Background:** This study aimed to define the distribution and frequency of fracture lines and bone defects in displaced femoral neck fractures (DFNFs) using a three-dimensional (3D) mapping technique, and to investigate the factors associated with the area of bone defects in patients with DFNFs.

**Methods:** The data of 256 adult patients with DFNFs were retrospectively reviewed. Multiplanar reconstructions of the DFNFs were made using computed tomography (CT) images, and the DFNF fragments were virtually reduced to match a 3D model of the femoral neck. Subsequently, 3D mapping was performed by graphically superimposing all of the fracture lines and bone defects onto a femoral neck template. The 3D mappings were independently examined by two orthopedic surgeons, and the interobserver agreement was analyzed. For intraobserver analysis, one of the surgeons measured the mappings twice more, and the intraclass correlation coefficients (ICCs) were calculated. A linear regression analysis was conducted to explore bone defect area-related factors.

**Results:** The cohort comprised 141 (55%) patients with left hip injuries and 115 (45%) patients with right hip injuries. On the 3D maps, the dense zones of the fracture lines were largely observed from the superior to the posterior part of the femoral neck, while the dense zone of the bone defect was primarily concentrated in the posterior part of the femoral neck. Only a few dense zones were located in the anterior and inferior parts of the femoral neck. An overlapping region between the fracture line and the bone defect was located in the 2.5th to 4.5th (5th) part of the 1/10 of the superior (posterior) femoral neck length. Both the fracture line and bone defect mapping techniques had good intra- and inter-observer reliability, with ICCs of 0.879 (0.977) and 0.780 (0.974), respectively. Garden type and age were positively correlated with bone defects, while simplified AO Foundation/Orthopaedic Trauma Association (AO/OTA) classification was negatively associated with bone defects.

**Conclusions:** The fracture lines and bone defects of the DFNFs were mainly located in the superior and posterior parts of the femoral neck, while an overlapping region was observed in the subcapital area of the femoral neck. 3D mapping is a reliable method for searching for DFNF features, and separately studying fracture lines and bone defects can further elucidate the morphology of these fractures. Bone defects in patients with DFNFs were associated with Garden type, simplified AO/OTA classification, and age.

^ ORCID: Shenghui Wu, 0000-0002-2218-0642; Xiaozhong Zhu, 0000-0002-1582-9423; Wei Wang, 0000-0001-8487-444X; Yingqi Zhang, 0000-0002-4616-6888; Guangyi Li, 0000-0003-4487-4386; Jiong Mei, 0000-0003-2290-3238.

**Keywords:** Femoral neck fracture (FNF); 3D mapping; reliability analysis; bone defect; age

Submitted Mar 07, 2022. Accepted for publication Jul 28, 2022.
doi: 10.21037/atm-22-1213
**View this article at:** https://dx.doi.org/10.21037/atm-22-1213

## Introduction

Femoral neck fractures (FNFs) are common in the clinical setting, and the incidence of FNFs is increasing with the aging population (1). These fractures can be divided into non-displaced or displaced fractures, with the latter accounting for about two-thirds of FNFs (2). The surgical treatment of displaced femoral neck fractures (DFNFs) has posed significant challenges for centuries. Operative options for DFNFs include internal fixation and hip arthroplasty; however, the best surgical management for DFNFs remains controversial (3). Given the complications associated with joint replacement, such as aseptic loosening, and the limited longevity of prostheses, internal fixation is generally prioritized in surgery (4).

The success of the internal fixation of DFNFs is largely dependent on two factors: anatomic reduction and internal fixation stability. Reducing a fracture usually depends on its pattern, and unstable types of fracture may create difficulties in fracture reduction (5). Bone defect or comminution is an important factor for unstable fracture and fixation instability in patients with FNFs (6). Additionally, malreduction and fixation instability may prevent normal fracture healing (7,8). Thus, insights into the morphological characteristics of fracture lines and bone defects will improve the understanding of DFNFs, which may aid in enhancing preoperative planning, intraoperative surgical techniques, and mechanical study models (9). At present, age is established as an important factor in clinical decision-making for patients with DFNFs; however, the relationships of age and other parameters with morphological features of DFNFs have yet to be elucidated.

To address this gap in the knowledge, the present study aimed to define the distribution and frequency of fracture lines and bone defects in DFNFs using a three-dimensional (3D) mapping technique, and to investigate factors for the area of bone defects in patients with DFNFs. We hypothesized that reliable mapping techniques would reveal consistent fracture patterns and bone defects in patients with DFNFs, and that factors related to bone defect area would include age and fracture classification. We present the following article in accordance with the STROBE reporting checklist (available at https://atm.amegroups.com/article/view/10.21037/atm-22-1213/rc).

## Methods

### *Participants*

This retrospective study was conducted in accordance with the Declaration of Helsinki (as revised in 2013). The study was approved by the Human Research Ethics Committee of Shanghai Sixth People's Hospital before participant enrolment [No. 2020-KY-026(K)], and the requirement for individual consent for this retrospective study was waived.

To identify patients for inclusion in the study, we conducted a retrospective search of a prospectively maintained orthopedic database at a large level-I trauma center to retrieve computed tomography (CT) imaging data of patients diagnosed with FNFs between December 2017 and December 2019. A total of 399 adult patients with FNFs were consecutively enrolled in this study. Patients were included in the study if they were aged over ≥18 years and had a DFNF (Garden III–IV). Patients who had axial CT images with a slice thickness of >1 mm, pathological fractures, bilateral FNFs, or congenital or acquired malformations of the femoral neck were excluded from the study. Ultimately, 256 DFNFs from 256 patients were included in the analysis. The Garden type and Pauwels angle of each patient were identified by two orthopedic surgeons, and any discrepancies that arose between the pair were resolved by a third orthopedic surgeon.

### *Radiological analysis*

The CT data of the DFNFs of all patients in Digital Imaging and Communications in Medicine (DICOM) format were acquired from a picture archiving and communication system workstation. Raw images were transferred into Mimics 17.0 software (Materialise, Leuven, Belgium). The DFNF fragments were segmented by masking the CT threshold ranges associated with each

 

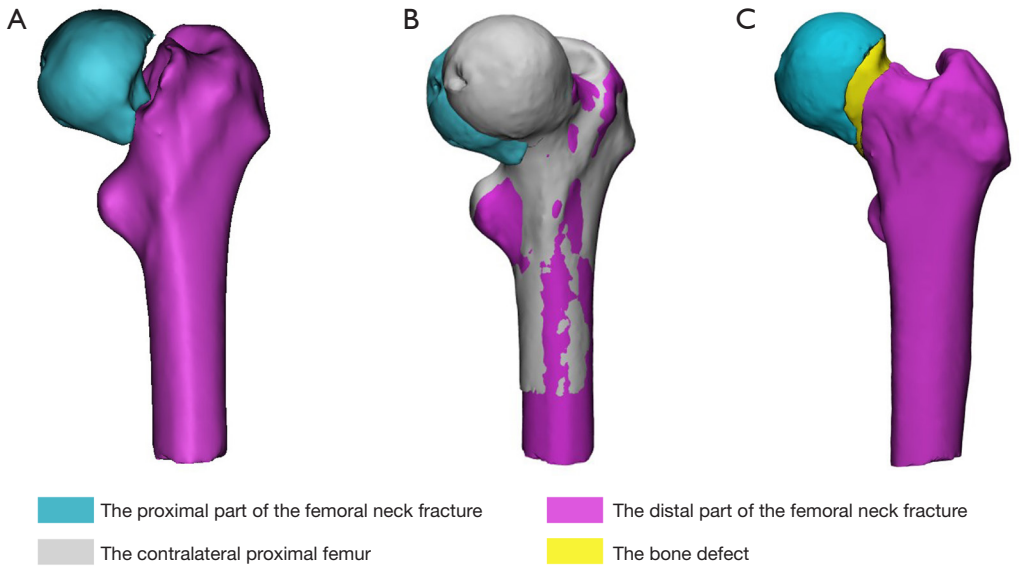


**Figure 1** The process of virtual reduction. (A) Three-dimensional model of fracture fragments of displaced FNFs; (B) the best possible alignment between the bilateral femur, except for the proximal part of the FNF; (C) a fracture fragment model after reduction. FNF, femoral neck fracture.

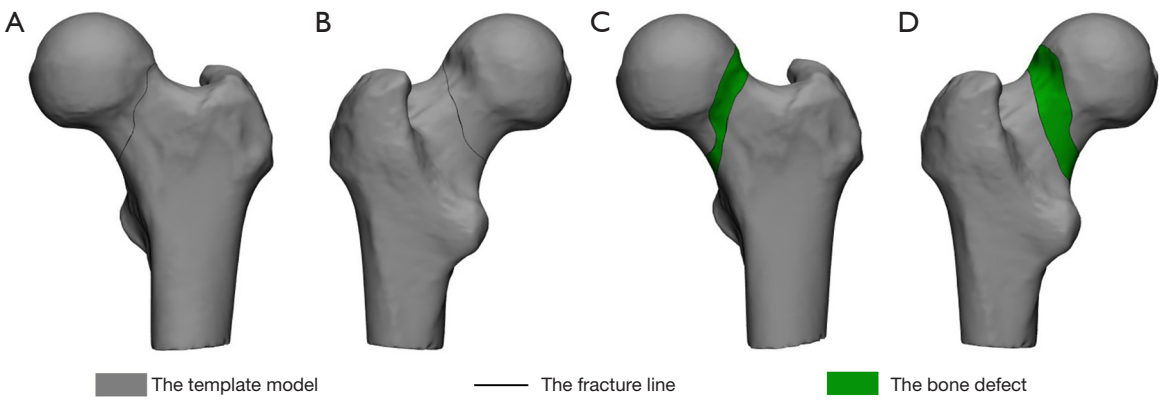


**Figure 2** Projection of the fracture line and bone defect to the standard template. (A) The anterior view of the fracture line; (B) the posterior view of the fracture line; (C) the anterior view of the bone defect; (D) the posterior view of the bone defect.

fragment based on the general principle of the segmentation (10-12), and multiplanar reconstructions were performed using Mimics.

### *Virtual reduction*

The data were subsequently exported into the 3-matic 10.0 software (Materialise). The DFNF fragments were virtually reduced, with the contralateral proximal femur as a standard (*Figure 1*).

### *3D mapping of fracture lines and bone defects*

The reconstructed models were rotated, normalized, and horizontally flipped, as necessary, to best match a 3D model of the proximal femur. Smooth curves were delineated precisely on the template surface to reproduce the fracture line and bone defect distribution of each DFNF in 3-matic, and the area of the proximal site of the fracture line and the bone defect was determined separately (*Figure 2*). The graphical superimpositions of the fracture lines and bone defects of all the patients were transferred to e-3D

 

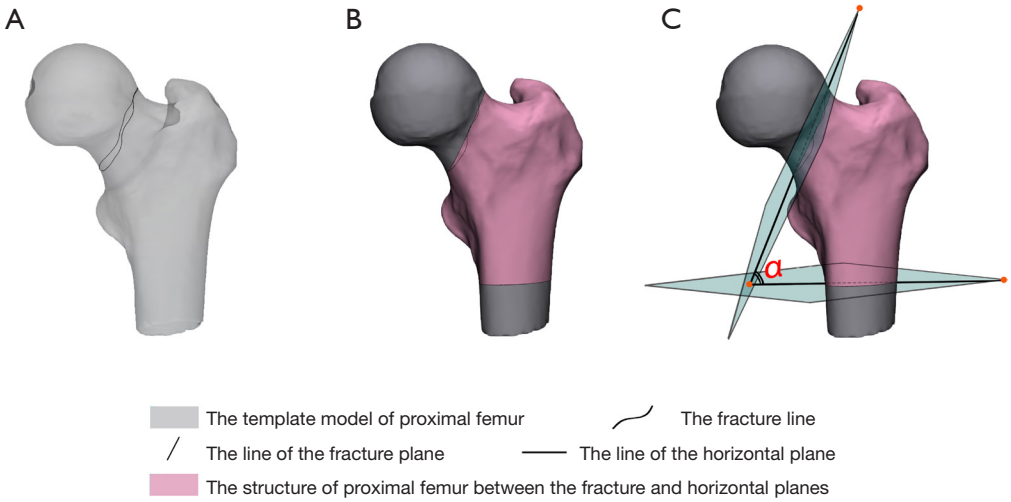


**Figure 3** Three-dimensional measurement of a Pauwels angle. (A) Three-dimensional visualization of the fracture line; (B) the horizontal plane and fracture plane defined as the best-fit plane of the fracture line; (C) three-dimensional visualization of the Pauwels angle (α).

software (Central South University, Changsha, China) and transformed into stereo fracture maps. The 3D heat maps indicated the relative frequency of the fracture lines using colors (ranging from blue to red, indicating a low to high incidence, respectively). To better delineate the dense fracture zones in the femoral neck, the length of the femoral neck was divided into 10 equal deciles.

### *Measurement of Pauwels angle based on the fracture line*

The measurement principle adopted to determine the Pauwels' angle was based on a previously described method (13). The Pauwels angle in each 3D model was defined as the angle between the fracture plane and the horizontal plane. The fracture plane was determined according to the best-match-similarity plane of the fracture line. The horizontal plane was defined as being perpendicular to the femoral shaft (*Figure 3*).

### *Reliability analysis of the 3D mapping*

To determine the sample size needed to analyze the reliability of the 3D mapping, *a priori* power analysis was performed. To ensure good reliability, the sample size calculation was performed using PASS15.0.5 (NCSS, LLC. Kaysville, Utah) with a power of 90% and an α value of 0.05 for the two observers as follows: ρ0=0.75 (14) and ρ1=0.885 (0.946). The value of ρ1 was obtained from the pre-test on fracture lines (bone defects). Thus, we determined that the minimum required sample size for the observer reliability analysis was 49 patients.

Each CT image of all 49 randomly selected patients was shown individually to the two authors. For the interobserver analysis, the two observers independently mapped each model using the 3D mapping technique. For the intraobserver analysis, 3D mapping was conducted twice more at 1-month intervals by one of the observers.

### *Statistical analysis*

Qualitative data were expressed as the number (percentage), and quantitative data were expressed as the mean (standard deviation). All analyses were performed using SPSS 24.0 software (IBM SPSS Inc., Armonk, NY, USA). Patients aged ≥65 years were defined as the older group. Differences between groups were analyzed using the chi-squared test or Fisher's exact probability method for dichotomized values and the Mann-Whitney test for continuous values. To assess intra- and interobserver reliability, the intraclass correlation coefficients (ICCs) were calculated based on the area of fracture regions on the models using a two-way random-effects model with absolute agreement. The ICCs were interpreted according to a method proposed by Landis and Koch (15). Univariate regression models were used to determine the significance of various factors, including the injured side, age, sex, the Pauwels angle, and different fracture classifications; significant factors were included in the multivariate regression model. Next, all the regression

 

models were adjusted for the baseline variables to investigate the factors related to the area of the bone defects. A P value <0.05 was considered statistically significant. A descriptive analysis was conducted of the fracture line and bone defect distributions.

## Results

### *Patient characteristics*

The cohort comprised 256 patients. The patient characteristics and the features of the DFNFs are summarized in *Table 1*. There were significant differences in many factors between the adult patient and older patient groups (*Table 1*).

### Intra- and interobserver reliability

In relation to the fracture line mapping, the results showed substantial interobserver and almost perfect intraobserver reliability, with ICCs of 0.780 [95% confidence interval (CI): 0.640–0.870] and 0.879 (95% CI: 0.796–0.930), respectively. Additionally, as evidenced by ICCs of 0.974 (95% CI: 0.0.955–0.985) and 0.977 (95% CI: 0.960–0.987), the inter- and intraobserver reliability for the bone defect mapping was almost perfect.

### Linear regression analysis

*Table 2* presents the results of univariate analysis of factors related to the area of bone defects in the patients with DFNFs. The multivariate linear regression models showed that the area of bone defects in the DFNFs was associated with Garden type and simplified AO Foundation/ Orthopaedic Trauma Association (AO/OTA) classification (*Table 3*). Additionally, the multivariate linear regression analysis revealed a statistically significant association between bone defects and age in all patients (P<0.001). In the older group, bone defects were correlated with Garden type (*Table 4*), while in the adult group, they were correlated with Garden type, Pauwels classification, and simplified AO/OTA classification (*Table 5*).

### *3D mapping of fracture lines*

Most of the fracture lines were located in the subcapital area of the femoral neck. The fracture lines ran in a trajectory along half of the anterior, one-third of the superior, one-third of the posterior, and half of the inferior parts of the femoral neck (*Figure 4*). As shown by the heatmap in *Figure 5*, the densest zone for fracture lines was in the superior site and the second densest zone was in the posterior site.

### *3D mapping of bone defects*

Most of the bone defects were located in the medial three-quarters of the sub-capital area of the femoral neck and were only sparsely distributed in the inferior area (*Figure 6*). As shown by the heatmap in *Figure 7*, the densest zone for bone defects was in the posterior site and the second densest zone was in the superior site; only a few dense zones were observed in the anterior and inferior parts of the femoral neck.

The fracture lines were mainly distributed from the 2.5$^{th}$ to the 4.5$^{th}$ and the 5$^{th}$ of the 1/10 part of the superior and posterior femoral neck length, while the bone defects were mainly located in the 2$^{nd}$ to the 7$^{th}$ part and the 3$^{rd}$ to the 6$^{th}$ of the 1/10 part of the superior and posterior femoral neck length. The overlapping area for the fracture lines and bone defects was mainly located in the dense zone for the fracture lines; however, the area of the dense zone for bone defects was larger than that for fracture lines (*Figure 8*).

## Discussion

Our results using reliable mapping techniques in patients with DFNFs showed consistent fracture lines in the femoral neck and that bone defects were associated with Garden type, simplified AO/OTA classification, and age, thus confirming our hypothesis. The consistent distribution of fracture lines in the femoral neck in the present study corresponds well with those in previous fracture mapping studies on different fracture sites (16,17). Additionally, advanced CT imaging analysis of the fracture lines and bone defects of patients with DFNFs revealed several important morphological characteristics that had not previously been identified. The method for analyzing interobserver reliability of fracture mapping has been established, and fracture mapping has been combined with quantitative evaluation of bone defect areas to explore related factors and improve the understanding of DFNFs, which in turn has enhanced the treatment of unstable and comminuted fractures (18). We found that bone defects were independent of the Pauwels angle, with related classification, in all patients with DFNFs, and bone defects were independent of age in both the adult and the older patient groups.

In this study, the use of 3D mapping techniques

 

**Table 1** Background characteristics of patients with DFNFs

| Characteristics | Total | Adult group | Older group | P value |
|---|---|---|---|---|
| Side of injury, n (%) | | | | 0.519* |
| Left | 141 (55.1) | 67 (57.3) | 74 (53.2) | |
| Right | 115 (44.9) | 50 (42.7) | 65 (46.8) | |
| Age (year) | 66.2±15.3 | 52.5±9.9 | 77.6±7.9 | <0.001#,^ |
| Sex, n (%) | | | | <0.001*,^ |
| Male | 120 (46.9) | 69 (59.0) | 51 (36.7) | |
| Female | 136 (53.1) | 48 (41.0) | 88 (63.3) | |
| Diameter of femoral head (mm) | 46.54±3.65 | 47.59±3.78 | 45.66±3.31 | <0.001#,^ |
| Garden type, n (%) | | | | 0.130* |
| III | 170 (66.4) | 72 (61.5) | 98 (70.5) | |
| IV | 86 (33.6) | 45 (38.5) | 41 (29.5) | |
| Pauwels angle (°) | 53.98±10.08 | 56.41±10.35 | 51.93±9.40 | 0.001#,^ |
| Pauwels classification, n (%) | | | | 0.002†,^ |
| Pauwels 1 (<30°) | 1 (0.4) | – | 1 (0.7) | |
| Pauwels 2 (30°–50°) | 99 (38.7) | 33 (28.2) | 66 (47.5) | |
| Pauwels 3 (>50°) | 156 (60.9) | 84 (71.8) | 72 (51.8) | |
| Simplified AO/OTA classification, n (%) | | | | <0.001*,^ |
| 32B1.3 | 75 (29.3) | 25 (21.4) | 50 (36.0) | |
| 31B2.1 | 55 (21.5) | 18 (15.4) | 37 (26.6) | |
| 31B2.2 | 61 (23.8) | 31 (26.5) | 30 (21.6) | |
| 31B2.3 | 65 (25.4) | 43 (36.8) | 22 (15.8) | |
| AO/OTA classification, n (%) | | | | <0.001†,^ |
| 31B1.3 | 75 (29.3) | 25 (21.4) | 50 (36.0) | |
| 31B 2.1q | 53 (20.7) | 16 (13.7) | 37 (26.6) | |
| 31B 2.1r | 2 (0.8) | 2 (1.7) | – | |
| 31B 2.2p | 1 (0.4) | – | 1 (0.7) | |
| 31B 2.2q | 59 (23.1) | 30 (25.6) | 29 (20.9) | |
| 31B 2.2r | 1 (0.4) | 1 (0.9) | – | |
| 31B 2.3q | 50 (19.5) | 33 (28.2) | 17 (12.2) | |
| 31B 2.3r | 15 (5.9) | 10 (8.5) | 5 (3.6) | |
| Bone defect area ($cm^2$) | 11.40±5.14 | 10.01±4.08 | 12.56±5.64 | <0.001#,^ |

*, P values determined using the chi-square test when comparing differences between the adult group and the older adult group; #, P values derived using the Mann-Whitney test when comparing difference between the adult group and the older adult group; †, P values determined using Fisher's exact test when comparing differences between the adult group and the older adult group; ^, P<0.05 was considered significant. p, Pauwels angle <30°; q, 30°≤ Pauwels angle ≤70°; r, Pauwels angle >70°. DFNF, displaced femoral neck fracture; AO/OTA, AO Foundation/Orthopaedic Trauma Association.

**Table 2** Results of univariate linear regression analysis for all DFNFs

| Variable | β value | 95% CI | P value |
|---|---|---|---|
| Side | 0.375 | −0.898 to 1.648 | 0.563 |
| Age* | 0.094 | 0.054 to 0.134 | <0.001 |
| Sex* | 1.366 | 0.107 to 2.624 | 0.034 |
| Diameter of femoral head | −0.137 | −0.310 to 0.035 | 0.119 |
| Garden type* | 3.279 | 2.000 to 4.558 | <0.001 |
| Pauwels angle* | −0.069 | −0.132 to −0.007 | 0.029 |
| Pauwels classification | | | |
| Pauwels I (<30°) | | Reference | |
| Pauwels II (30°–50°) | −0.216 | −10.349 to 9.918 | 0.967 |
| Pauwels III (>50°) | −1.503 | −11.618 to 8.612 | 0.770 |
| Simplified AO/OTA classification* | | | |
| 32B1.3 | | Reference | |
| 31B2.1 | −2.741 | −4.477 to −1.005 | 0.002 |
| 31B2.2 | −2.469 | −4.155 to −0.783 | 0.004 |
| 31B2.3 | −3.661 | −5.318 to −2.004 | <0.001 |
| AO/OTA classification | | | |
| 31B1.3 | | Reference | |
| 31B 2.1q | −2.733 | −4.491 to −0.976 | 0.002 |
| 31B 2.1r | −2.941 | −9.959 to 4.077 | 0.410 |
| 31B 2.2p | −1.107 | −10.967 to 8.753 | 0.825 |
| 31B 2.2q | −2.365 | −4.070 to −0.661 | 0.007 |
| 31B 2.2r | −9.931 | −19.791 to −0.071 | 0.048 |
| 31B 2.3q | −3.97 | −5.759 to −2.182 | <0.001 |
| 31B 2.3r | −2.63 | −5.400 to 0.141 | 0.063 |

*, represents a related factor with a statistically significant difference (P<0.05). p, Pauwels angle <30°; q, 30°≤ Pauwels angle ≤70°; r, Pauwels angle >70°. DFNF, displaced femoral neck fracture; CI, confidence interval; AO/OTA, AO Foundation/Orthopaedic Trauma Association.

**Table 3** Results of multivariate linear regression analysis for all the DFNFs—adjusted for age and sex

| Variable | β value | 95% CI | P value |
|---|---|---|---|
| Pauwels angle | −0.04 | −0.102 to 0.022 | 0.208 |
| Garden type | 3.562 | 2.345 to 4.780 | <0.001 |
| Simplified AO/OTA classification | | | |
| 31B 1.3 | | Reference | |
| 31B 2.1 | −2.553 | −4.244 to −0.863 | 0.003 |
| 31B 2.2 | −1.757 | −3.433 to −0.082 | 0.040 |
| 31B 2.3 | −3.01 | −4.65 to −1.37 | <0.001 |

DFNF, displaced femoral neck fracture; CI, confidence interval; AO/OTA, AO Foundation/Orthopaedic Trauma Association.

proved to be reliable. The 3D maps of the fracture lines and bone defects were presented separately to support a better understanding of the fracture morphologies. 3D mapping techniques have previously been used to study the morphological characteristics of fractures (including fractures of the patella, tibial plateau, distal femur, and scapula), suggest new surgical approaches, and develop fixation innovations to better address complex injuries (9,16). However, while 3D fracture mapping techniques are recognized and well accepted, previous studies have not examined the reliability of this evaluation method. Furthermore, previous studies used fracture lines to elucidate the dense zones of fracture lines and bone defects, or fracture comminutions, and this method may be prone to bias. Our study demonstrated that the 3D mapping of fracture lines and bone defects in DFNFs is a reliable method with good inter- and intraobserver reliability, with the area of the dense zone being larger for bone defects than for fracture lines. Thus, this technique could be used to depict the features of complex injuries. Additionally, a separate mapping study of fracture lines and bone defects was conducted to better characterize the morphological features of fractures.

Clinical decision-making about whether to perform hip replacements for DFNFs takes into account age and other potential predictors of bone defects. Our study showed that Garden type and age were positively correlated with bone defects, whereas simplified AO/OTA classification was negatively associated with bone defects. Thus, older DFNF patients and those classified as Garden type IV or AO/OTA class 31B1.3 may have more significant bone defects. Previous studies have shown that age is the primary independent risk factor for fixation failure in patients with FNFs and that Garden type is a significant risk factor for osteonecrosis after internal fixation (19,20). Comminution, especially posterior comminution, is also associated with high risks of mechanical failure and non-union for FNFs (21). Thus, hip replacement may be a reasonable therapeutic option for older patients diagnosed with DFNFs classified as Garden type IV or AO/OTA class 31B1.3 (22).

 

**Table 4** Results of univariate linear regression analysis for the DFNFs in the older adult group

| Variable | β value | 95% CI | P value |
|---|---|---|---|
| Side | 1.037 | −0.858 to 2.932 | 0.281 |
| Age | 0.090 | −0.029 to 0.210 | 0.137 |
| Sex | 0.924 | −1.040 to 2.888 | 0.354 |
| Diameter of femoral head | −0.024 | −0.312 to 0.264 | 0.868 |
| Garden type | 5.483 | 3.618 to 7.347 | <0.001 |
| Pauwels angle | −0.039 | −0.140 to −0.063 | 0.453 |
| Pauwels classification | | | |
| Pauwels I (<30°) | | Reference | |
| Pauwels II (30°–50°) | 0.113 | −11.208 to 11.434 | 0.984 |
| Pauwels III (>50°) | 0.217 | −11.096 to 11.531 | 0.970 |
| Simplified AO/OTA classification | | | |
| 32B1.3 | | Reference | |
| 31B2.1 | −2.796 | −5.162 to −0.429 | 0.021 |
| 31B2.2 | −1.867 | −4.388 to −0.653 | 0.145 |
| 31B2.3 | −3.719 | −6.511 to −0.926 | 0.009 |
| AO/OTA classification | | | |
| 31B1.3 | | Reference | |
| 31B 2.1q | −2.796 | −5.180 to −0.411 | 0.022 |
| 31B 2.2p | −1.902 | −13.008 to 9.204 | 0.735 |
| 31B 2.2q | −1.866 | −4.433 to −0.701 | 0.153 |
| 31B 2.3q | −3.630 | −6.717 to −0.542 | 0.022 |
| 31B 2.3r | −4.021 | −9.179 to 1.137 | 0.125 |

p, Pauwels angle <30°; q, 30°≤ Pauwels angle ≤70°; r, Pauwels angle >70°. DFNF, displaced femoral neck fracture; CI, confidence interval; AO/OTA, AO Foundation/Orthopaedic Trauma Association.

**Table 5** Results of univariate linear regression analysis for the DFNFs in the adult group

| Variable | β value | 95% CI | P value |
|---|---|---|---|
| Side | −0.652 | −2.163 to 0.859 | 0.395 |
| Age | 0.071 | −0.004 to 0.146 | 0.063 |
| Sex | 0.747 | −0.772 to 2.265 | 0.332 |
| Diameter of femoral head | −0.072 | −0.270 to 0.127 | 0.477 |
| Garden type | 1.563 | 0.049 to 3.077 | 0.043 |
| Pauwels angle | −0.049 | −0.121 to 0.024 | 0.186 |
| Pauwels classification | −2.105 | −3.725 to −0.484 | 0.011 |
| Simplified AO/OTA classification | | | |
| 32B1.3 | | Reference | |
| 31B2.1 | −2.673 | −5.125 to −0.221 | 0.033 |
| 31B2.2 | −2.230 | −4.363 to −0.098 | 0.041 |
| 31B2.3 | −2.449 | −4.444 to −0.454 | 0.017 |
| AO/OTA classification | | | |
| 31B1.3 | | Reference | |
| 31B 2.1q | −2.838 | −5.355 to −0.321 | 0.027 |
| 31B 2.1r | −1.352 | −7.129 to 4.425 | 0.644 |
| 31B 2.2q | −2.027 | −4.156 to −0.102 | 0.062 |
| 31B 2.2r | −8.342 | −16.359 to −0.325 | 0.042 |
| 31B 2.3q | −2.966 | −5.051 to −0.882 | 0.006 |
| 31B 2.3r | −0.742 | −3.684 to 2.199 | 0.618 |

q, 30°≤ Pauwels angle ≤70°; r, Pauwels angle >70°. DFNF, displaced femoral neck fracture; CI, confidence interval; AO/OTA, AO Foundation/Orthopaedic Trauma Association.

Our study also showed that Pauwels-related characteristics, including the Pauwels angle and Pauwels classification, and AO/OTA classification were not correlated with bone defects in DFNFs.

Developed in 1935, the Pauwels classification was the first biomechanical classification for FNFs that evaluated shearing stress and compressive force (13). A bone defect caused by an interplay of forces between fracture fragments may be dissipated by fracture displacement and varus collapse resulting from shearing forces. Thus, the Pauwels classification is not a predictor of bone defects in DFNFs, but both Pauwels classification and bone defects, or total comminutions, are two critical elements in instability assessments of DFNFs (20). Further, our results showed that many factors differed between the adult and older patient groups. As per the results of the subgroup analysis, Garden type, Pauwels classification, and simplified AO/OTA classification should be seriously considered for adult patients with DFNFs, while Garden type should be carefully considered for older patients.

An improved understanding of DFNF morphology could assist in the evaluation of the general underlying injury mechanism and intraoperative reduction. In this study, fracture line mapping demonstrated that the initial fracture sites were located mainly in the superior site of the femoral neck, while the force was transmitted mainly

 

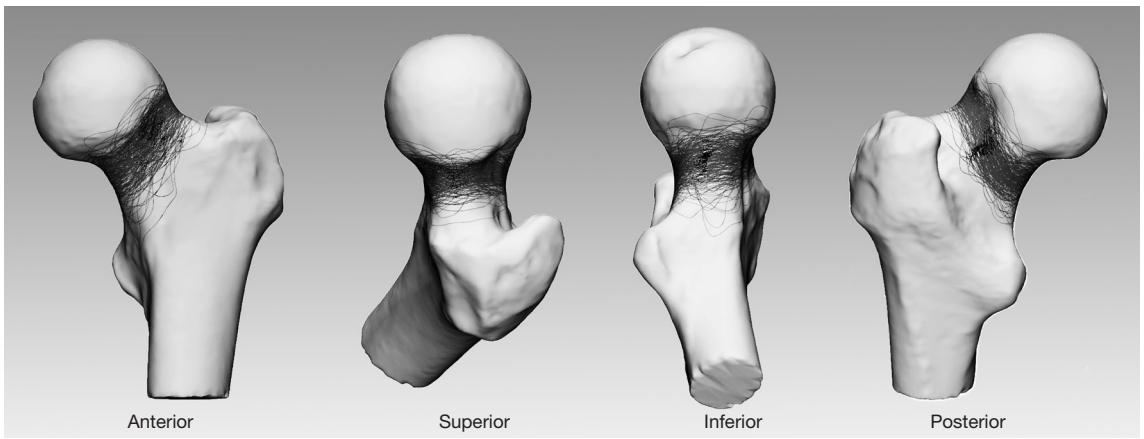


**Figure 4** Representative views of three-dimensional mapping of all the fracture lines for the displaced femoral neck fractures, including the anterior, superior, inferior, and posterior views.

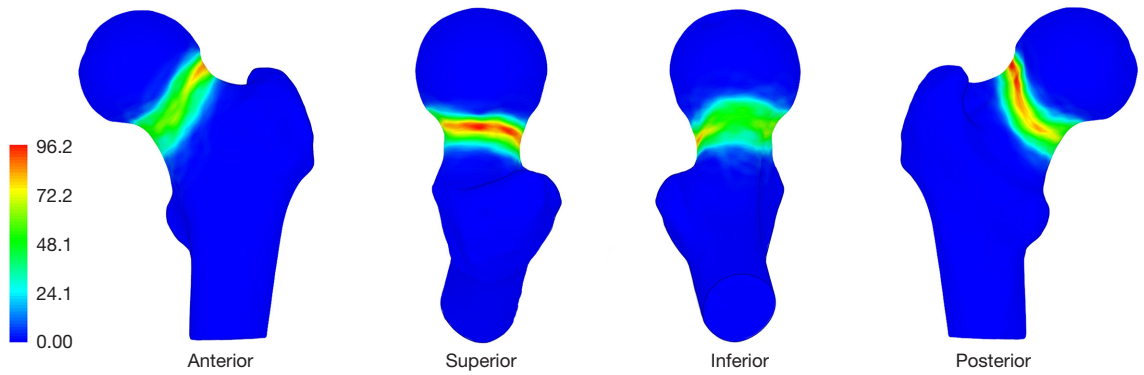


**Figure 5** Representative views of three-dimensional heat mapping of all the fracture lines for the displaced femoral neck fractures, including the anterior, superior, inferior, and posterior views.

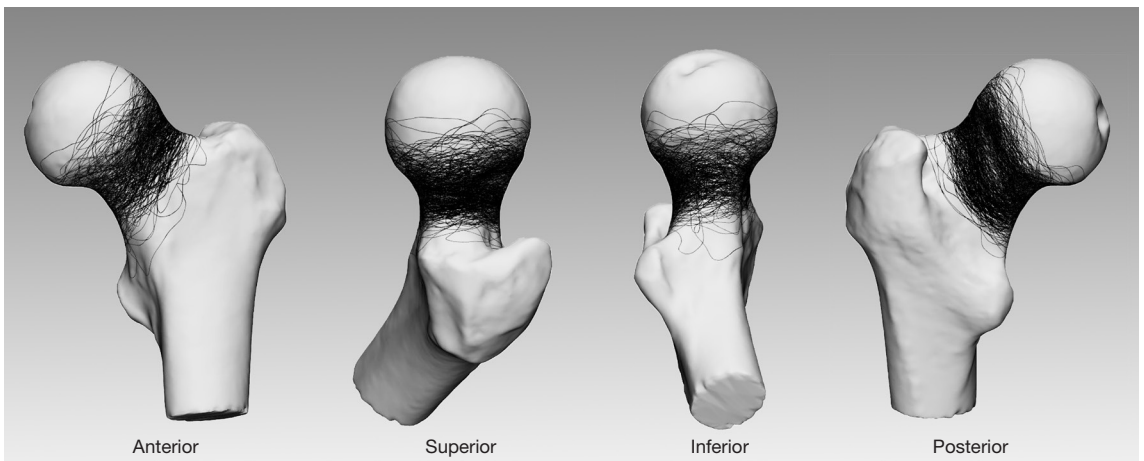


**Figure 6** Representative views of the three-dimensional mapping of all the bone defects for the displaced femoral neck fractures, including the anterior, superior, inferior, and posterior views.

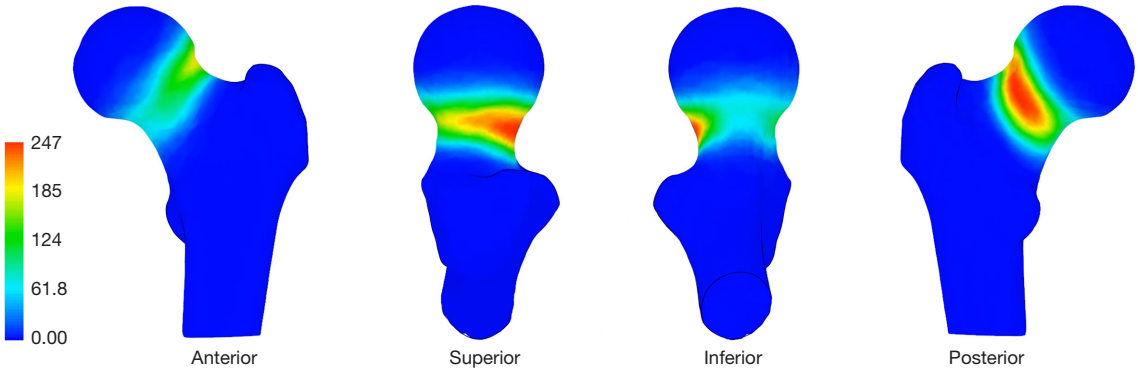


**Figure 7** Representative views of the three-dimensional heat mapping of all the bone defects for the displaced femoral neck fractures, including the anterior, superior, inferior, and posterior views.

along the superior site to the posterior site. Additionally, our study revealed that the distribution of bone defects mainly occurred in the posterior site of the femoral neck and extended to the superior site. The changes in the displacement of fracture fragments changed with the shearing stress and compressive force. However, fracture displacement elicits difficulties in reduction, which in turn results in a poor prognosis (23); thus, the addition of internal rotation traction would improve appropriate preoperative care and surgical management (24). Additionally, due to the sparse distributions of fracture lines and bone defects in the anterior and superior sites of the femoral neck, anterior and inferior cortical apposition patterns could aid intraoperative evaluations in DFNF reduction based on X-rays.

The morphologic fracture characteristics identified in our study may improve the development of surgical concepts relative to DFNFs. Unlike previous work (18) in which the degree of bone defects or the total comminutions associated with DFNFs may have been underestimated, our results, which were obtained using our method of 3D fracture analysis, revealed bone defects in the DFNFs located in the posterior and superior site of the femoral neck. Posterior comminution is a significant factor for insecure fixation in DFNFs. Different internal fixations combined with posterior bone grafting can be used to provide stability for DFNFs; however, the non-union rate is still between 10% and 20% (18). Thus, the superior site and overlapping region of the fracture line and bone defect need adequate attention. Stress mainly occurs in the overlapping area, which results in the generation of cracks and comminutions.

The fracture maps generated in this study could also aid in the evaluation of vascular damage to the femoral head of patients with DFNFs. The absence of nutrient foramina in the fovea capitis femoris has been shown to be associated with a high likelihood of femoral head osteonecrosis (25). Thus, a residual blood supply around the femoral head and neck junction is crucial for patients with DFNFs, especially when nutrient foramina are absent from the fovea capitis femoris. Our study showed that the region of bone defects in DFNFs is partly located in the superior site of the femoral neck. Loss of blood supply in the superior site of the femoral neck increases the risk of avascular necrosis of the femoral head (26). Furthermore, fracture healing is based on two main factors: blood supply and stability (27). The current surgical techniques cannot completely reverse insufficient blood supply to the femoral head; thus, much greater emphasis on the stability of internal fixation is required. The overlapping area of the fracture line and bone defect could be a potential weak area. To improve the stability of fracture fixation, a bone graft is necessary to fill the dense zones of the fracture line and bone defect, especially the overlapping area.

This study had some limitations. First, these findings may improve the understanding of the general principles of fracture morphology, but further studies are needed to explore rare conditions. Second, due to the virtual reduction, 3D fracture mapping could only show the distribution of the fracture morphology on the proximal femur surface rather than the displacement and volume of the fragments of the DFNFs. More innovative imaging techniques are therefore needed to implement relevant research (28). Third, the reliability analysis of the Pauwels angle was not examined. However, a previous study

 

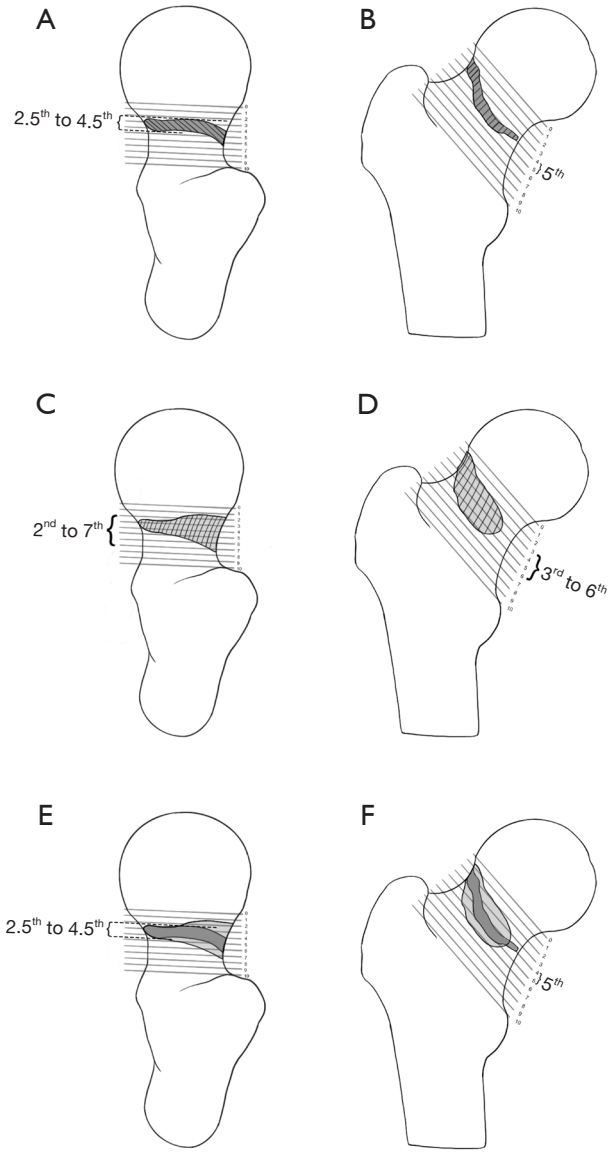


**Figure 8** Geometrical diagram of three-dimensional mapping of the displaced femoral neck fractures. To describe the position of the dense zones in the femoral neck, the length of the femoral neck was approximately divided into 10 equal deciles. (A) The superior view of the fracture line distribution mainly in the 2.5th to 4.5th parts; (B) the posterior view of the fracture line distribution mainly in the 5th part; (C) the superior view of the bone defect distribution mainly in the 2nd to 7th parts; (D) the posterior view of the bone defect distribution mainly in the 3rd to 6th parts; (E) the superior view of the overlapping region of the fracture line and bone defect distributions mainly in the 2.5th to 4.5th parts; (F) the posterior view of the overlapping region of the fracture line and bone defect distributions mainly in the 5th part.

demonstrated reliable 3D angle measurement based on CT images (29). Fourth, other factors related to bone defect area need to be assessed in biomechanics and clinical studies in the future.

## Conclusions

Our study has clarified the general morphological characteristics of DFNFs in 3D fracture maps and also assessed the reliability of a 3D fracture mapping technique. The fracture line and bone defect regions were mainly located in the superior and posterior sites of the femoral neck, and an overlapping area was distributed from the 2.5$^{th}$ to 4.5$^{th}$ and the 5$^{th}$ of the 1/10 part of the superior and posterior femoral neck length. This 3D mapping technique is a reliable method for searching for regularities of DFNFs, and the separate study of fracture lines and bone defects can better elucidate the morphology of fractures. Bone defects in patients with DFNFs were found to be associated with Garden type, simplified AO/OTA classification, and age.

## Acknowledgments

*Funding:* This work was supported by the National Natural Science Foundation of China (Nos. 81271991 and 12172224).

## Footnote

*Reporting Checklist:* The authors have completed the STROBE reporting checklist. Available at https://atm.amegroups.com/article/view/10.21037/atm-22-1213/rc

*Data Sharing Statement:* Available at https://atm.amegroups.com/article/view/10.21037/atm-22-1213/dss

*Peer Review File:* Available at https://atm.amegroups.com/article/view/10.21037/atm-22-1213/prf

*Conflicts of Interest:* All authors have completed the ICMJE uniform disclosure form (available at https://atm.amegroups.com/article/view/10.21037/atm-22-1213/coif). The authors have no conflicts of interest to declare.

*Ethical Statement:* The authors are accountable for all aspects of the work in ensuring that questions related

to the accuracy or integrity of any part of the work are appropriately investigated and resolved. This retrospective study was conducted in accordance with the Declaration of Helsinki (as revised in 2013). The study was approved by the Human Research Ethics Committee of Shanghai Sixth People's Hospital before participant enrolment [No. 2020-KY-026(K)], and the requirement for individual consent for this retrospective study was waived.



## References

1. Harvey NC, Kanis JA, Liu E, et al. Impact of population-based or targeted BMD interventions on fracture incidence. Osteoporos Int 2021;32:1973-9.
2. Bhandari M, Devereaux PJ, Einhorn TA, et al. Hip fracture evaluation with alternatives of total hip arthroplasty versus hemiarthroplasty (HEALTH): protocol for a multicentre randomised trial. BMJ Open 2015;5:e006263.
3. Fischer H, Maleitzke T, Eder C, et al. Management of proximal femur fractures in the elderly: current concepts and treatment options. Eur J Med Res 2021;26:86.
4. Zelle BA, Salazar LM, Howard SL, et al. Surgical treatment options for femoral neck fractures in the elderly. Int Orthop 2022;46:1111-22.
5. Fu CW, Chen JY, Liu YC, et al. Dynamic Hip Screw with Trochanter-Stabilizing Plate Compared with Proximal Femoral Nail Antirotation as a Treatment for Unstable AO/OTA 31-A2 and 31-A3 Intertrochanteric Fractures. Biomed Res Int 2020;2020:1896935.
6. Huang ZY, Su YH, Huang ZP, et al. Medial Buttress Plate and Allograft Bone-Assisted Cannulated Screw Fixation for Unstable Femoral Neck Fracture with Posteromedial Comminution: A Retrospective Controlled Study. Orthop Surg 2022;14:911-8.
7. Elliott DS, Newman KJ, Forward DP, et al. A unified theory of bone healing and nonunion: BHN theory. Bone Joint J 2016;98-B:884-91.
8. Wang G, Tang Y, Wu X, et al. Finite element analysis of a new plate for Pauwels type III femoral neck fractures. J Int Med Res 2020;48:300060520903669.
9. Sarfani S, Beltran MJ, Benvenuti M, et al. Mapping of Vertical Femoral Neck Fractures in Young Patients Using Advanced 2 and 3-Dimensional Computed Tomography. J Orthop Trauma 2021;35:e445-50.
10. Zoroofi RA, Sato Y, Sasama T, et al. Automated segmentation of acetabulum and femoral head from 3-D CT images. IEEE Trans Inf Technol Biomed 2003;7:329-43.
11. Krcah M, Székely G, Blanc R. "Fully automatic and fast segmentation of the femur bone from 3D-CT images with no shape prior," 2011 IEEE International Symposium on Biomedical Imaging: From Nano to Macro 2011:2087-90.
12. Gangwar T, Calder J, Takahashi T, et al. Robust variational segmentation of 3D bone CT data with thin cartilage interfaces. Med Image Anal 2018;47:95-110.
13. Shen M, Wang C, Chen H, et al. An update on the Pauwels classification. J Orthop Surg Res 2016;11:161.
14. Koo TK, Li MY. A Guideline of Selecting and Reporting Intraclass Correlation Coefficients for Reliability Research. J Chiropr Med 2016;15:155-63.
15. Landis JR, Koch GG. The measurement of observer agreement for categorical data. Biometrics 1977;33:159-74.
16. Zhan Y, Zhang Y, Xie X, et al. Three-dimensional fracture mapping of multi-fragmentary patella fractures (AO/OTA 34C3). Ann Transl Med 2021;9:1364.
17. Yin Y, Zhang R, Hou Z, et al. Fracture Mapping of Both-Column Acetabular Fractures. J Orthop Trauma 2022;36:e189-94.
18. Scheck M. The significance of posterior comminution in femoral neck fractures. Clin Orthop Relat Res 1980;(152):138-42.
19. Xu JL, Liang ZR, Xiong BL, et al. Risk factors associated with osteonecrosis of femoral head after internal fixation of femoral neck fracture:a systematic review and meta-analysis. BMC Musculoskelet Disord 2019;20:632.
20. Randelli F, Viganò M, Liccardi A, et al. Femoral neck fractures: Key points to consider for fixation or replacement a narrative review of recent literature. Injury 2021. doi: 10.1016/j.injury.2021.09.024.
21. Rawall S, Bali K, Upendra B, et al. Displaced femoral neck fractures in the young: significance of posterior comminution and raised intracapsular pressure. Arch Orthop Trauma Surg 2012;132:73-9.
22. HEALTH Investigators; Bhandari M, Einhorn TA, et al. Total Hip Arthroplasty or Hemiarthroplasty for Hip Fracture. N Engl J Med 2019;381:2199-208.

 

23. Wang Y, Ma JX, Yin T, et al. Correlation Between Reduction Quality of Femoral Neck Fracture and Femoral Head Necrosis Based on Biomechanics. Orthop Surg 2019;11:318-24.
24. Khurana B, Mandell JC, Rocha TC, et al. Internal Rotation Traction Radiograph Improves Proximal Femoral Fracture Classification Accuracy and Agreement. AJR Am J Roentgenol 2018;211:409-15.
25. Zhao K, Zhang F, Quan K, et al. Insufficient blood supply of fovea capitis femoris, a risk factor of femoral head osteonecrosis. J Orthop Surg Res 2021;16:414.
26. Wu S, Quan K, Wang W, et al. 3D Mapping of Bone Channel of Blood Supply to Femoral Head in Proximal Femur. Front Surg 2022;9:852653.
27. Hulth A. Current concepts of fracture healing. Clin Orthop Relat Res 1989;(249):265-84.
28. Yao X, Zhou K, Lv B, et al. 3D mapping and classification of tibial plateau fractures. Bone Joint Res 2020;9:258-67.
29. Wu S, Wang W, Zhang B, et al. A three-dimensional measurement based on CT for the posterior tilt with ideal inter-and intra-observer reliability in non-displaced femoral neck fractures. Comput Methods Biomech Biomed Engin 2021;24:1854-61.

(English Language Editors: L. Huleatt and J. Reynolds)

**Cite this article as:** Wu S, Zhu X, Wang W, Zhang Y, Li G, Mei J. Three-dimensional computed tomography mapping and clinical predictive factors for morphologic characterization of displaced femoral neck fractures. Ann Transl Med 2022;10(20):1096. doi: 10.21037/atm-22-1213

 